



Hierarchical Porous BaTiO₃ Nano-Hexagons as A Visible Light Photocatalyst

Harsha Bantawal and D Krishna Bhat*

Department of Chemistry, National Institute of Technology Karnataka, Surathkal, Mangalore-575025, India

*Corresponding author E-mail: denthajekb@gmail.com, kishan@nitk.edu.in

Abstract

Hierarchical porous BaTiO₃ nano-hexagons was synthesized via a simple hydrothermal route by using TiO₂ and Ba(OH)₂.8H₂O as starting materials under alkaline environment and its photocatalytic activity was evaluated under visible light by taking methylene blue (MB) as a model pollutant. The prepared BaTiO₃ was characterized by powder X-ray diffraction (XRD), X-ray photoelectron spectroscopy (XPS), field emission scanning electron microscopy (FESEM), energy dispersive X-rays analysis (EDX), high resolution transmission electron microscopy (HRTEM), Brunauer-Emmett-Teller (BET) analysis and diffused reflectance spectroscopy (DRS) techniques. It is noteworthy that the BaTiO₃ nano-hexagons exhibited significant photocatalytic activity towards the degradation of MB under visible light irradiation. This significant photocatalytic activity of BaTiO₃ under visible light is mainly attributed to the special morphology and formation of Ti³⁺ defects.

Keywords: Advanced oxidation process, Barium titanate, Hydrothermal, Perovskite, Photocatalysis, Titanium oxide

1. Introduction

Water is imperative to life. The major portion of the water is constituted by aquatic resources such as salted waters of oceans, seas and glaciers. About only 0.65% of the water total mass can be usable by man. Therefore, there is an imperative need of developing potent and eco-friendly techniques to treat waste waters. Advanced Oxidation Processes (AOPs) have been defined by Glaze et al.¹ play a vital role in the removal of persistent organic pollutants. Photocatalysis is an integral part of the AOPs has been commonly employed in the removal of persistent organic pollutants because of its zero waste scheme and biocompatibility.² As we know that nearly 43% of the solar irradiation energy corresponds to the visible light and nearly 7% of the energy corresponds to the UV light. Undeniably, the first generation TiO₂ is a prominent photocatalyst in the UV region, due to its wide band gap of 3.2 eV hamper its use in visible range. Therefore, there is an imperative need in extension of visible light response of wide band gap photocatalysts.

Perovskite alkaline earth titanates (ATiO₃, A= Ca, Ba, Sr) are found to exhibit compelling properties in various applications like photocatalytic degradation of organics, photocatalytic water splitting and photo reduction of carbon dioxide due to their wide band gap, excellent catalytic activity, excellent chemical stability and good biocompatibility.³ Barium titanate (BaTiO₃), a ternary metal titanate perovskite with a high dielectric constant and ferroelectric properties has been extensively investigated. It is also a very important semiconductor under UV light due to its band gap of 3.25 eV and its photocatalytic activity is hampered in visible light. Therefore, several probes have been explored in order to enhance the photocatalytic activity of BaTiO₃ such as surface sensitization, ion doping, noble metal loading and heterostructural strategy. On the other side morphology has an imperative impact on photocata-

lytic activity. Yingpu et al.⁴ studied the facet effect of Ag₃PO₄ sub-microcrystals on photocatalytic properties. They found that the morphology control of semiconductors enables selective exposure of photocatalytically active facets, which might be applicable in the design of highly efficient visible light active catalysts. Yan et. al.⁵ synthesized rod like CaTiO₃. They found that the band gap of CaTiO₃ with this special morphology was narrowed.

Hydrothermal method has been employed for the fabrication of perovskite oxide owing to its high purity, homogeneity, crystallinity, well defined morphology and controllable particle size.⁶ To the best of our knowledge there has been no work devoted to the photocatalytic performance of BaTiO₃ nano-hexagons under visible light irradiation. In this work, we have synthesized BaTiO₃ hydrothermally using TiO₂, Ba(OH)₂.8H₂O and NaOH as raw materials and the as synthesized sample was thoroughly characterized by XRD, FESEM, TEM, HRTEM, BET, XPS and UV-visible diffuse reflectance spectroscopic techniques. The as prepared BaTiO₃ showed narrowed band gap owing to its special morphology and Ti³⁺ defects. The photocatalytic activity of the as synthesized sample was evaluated by taking methylene blue (MB) as the target pollutant under visible light irradiation.

2. Materials and method

Titanium(IV) oxide, anatase, 99.6% (metal basis)-325 Mesh Powder was procured from Alfa Aesar, Barium Hydroxide Extra pure (octahydrate) was procured from Loba Chemie Pvt. Ltd. and NaOH pellets were procured from Finar limited. All the chemicals were used without further purification. All the reactions were carried out with Millipore water.

BaTiO₃ nanopowder was synthesized in a beaker by taking 0.5 g Titanium(IV) oxide powder, 1.75 g Barium Hydroxide (octahydrate) and 50 mL of 5M NaOH. The mixture was magnetically stirred for 20 minutes and then placed in an ultrasonic bath for 5

minutes. The resultant mixture was transferred to a 100 mL Teflon lined autoclave and heated to 120°C for 48 hours. The precipitated powders were cooled to room temperature and neutralized to pH 7 with the help of 5M HCl solution. Excess liquid was removed by decantation and the white precipitate obtained was recovered by centrifugation with water. Finally, the obtained solid was dried at 80°C overnight.

The structural characterization of the synthesized material was performed using an X-ray diffractometer (XRD, Rigaku) with monochromatic Cu-K α radiation ($\lambda = 0.154$ nm) at a scan rate of 2° per minute in the range of 5-80°. The surface morphology was observed using FESEM (Carl Zeiss), TEM (Fie Tecnai), HRTEM (Fie Tecnai). The elemental analysis of the synthesized material was performed by using EDX (Carl Zeiss) and X-ray photoelectron spectrometer (Kratos XSAM800) equipped with a standard monochromatic Al K α source. The specific surface area was determined using Brunauer-Emmett-Teller (BET) method (BEL SORP II, JAPAN) based on adsorption data in the relative pressure in the range of 0.05-0.03. The pore size distribution was determined using the Barrett-Joyner-Halenda (BJH) method applied to the desorption branch. Diffuse reflectance spectrum was recorded using UV-Visible diffuse reflectance spectrometer (DRS, Analytic Jena).

The photocatalytic activity of the synthesized material was evaluated by taking methylene blue (MB) solution using a photocatalytic reactor under ambient atmospheric conditions. The photocatalytic reactor was equipped with a high - pressure 250 W Hg vapour lamp operating at a wavelength of 410-700 nm was used as a source of visible light. In these experiments 100 mL of MB solution (5.5 mg L⁻¹) and photocatalyst (50 mg) were taken in to a 500 mL of pyrex glass beaker and magnetically stirred for 30 minutes in order to reach adsorption-desorption equilibrium of the catalyst. Then the solution was irradiated with visible light radiation. During photocatalytic studies, at regular intervals, 5 mL of the reacted MB solution was sampled out, centrifuged and the absorbance of the supernatant dye solution was measured using UV – visible spectrometer at 664 nm. The percentage of degradation of the dye was calculated as per equation (1).⁷

$$\text{Degradation \%} = [(A_0 - A_t)/A_0] \times 100 \quad (1)$$

Where, A_0 is the initial absorbance of dye solution and A_t is the absorbance at different intervals of time.

3. Results and Discussions

3.1. XRD Studies

Figure 1 shows the XRD patterns of the as prepared BaTiO₃. The diffraction peaks at 22.01°, 31.40°, 38.76°, 45.01°, 50.65°, 55.96° and 65.63° were ascribed to the (100), (110), (111), (200), (210), (211) and (220) crystal planes of BaTiO₃ and confirm well to JCPDS file no. 01-075-0461. The average crystal size of BaTiO₃ was found to be 40.74 nm which was calculated from Scherrer equation.⁸

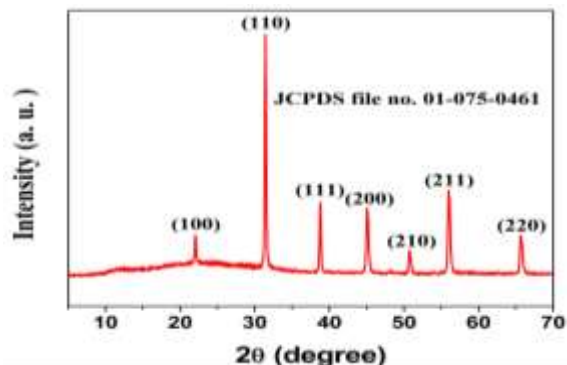


Fig. 1: XRD spectrum of BaTiO₃

3.2. BET Surface Area Analysis

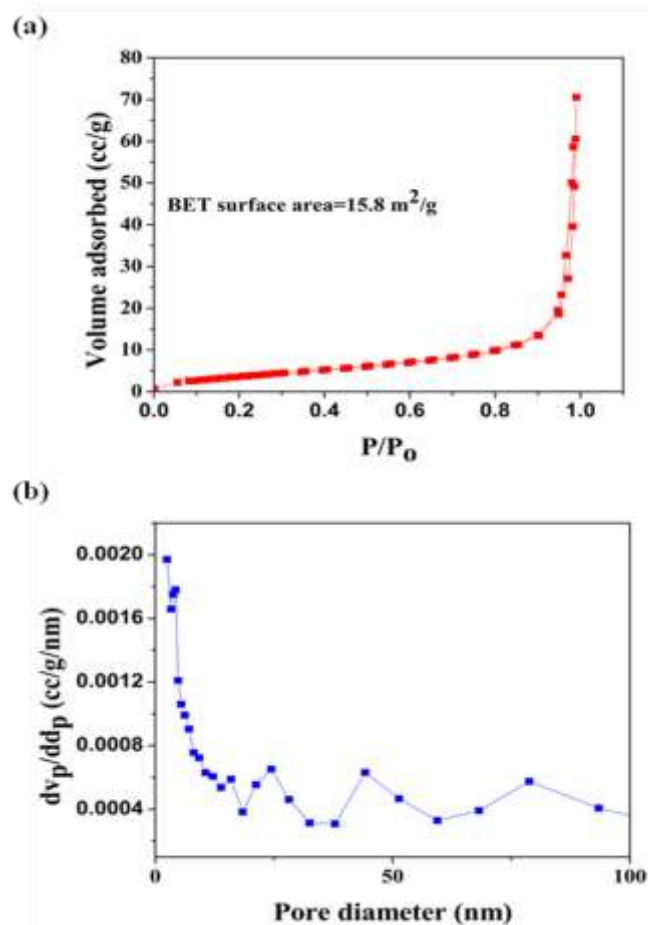


Fig. 2: BET surface area analysis: Adsorption-desorption isotherms

The nitrogen adsorption-desorption isotherms were used to obtain information about the BET specific surface area and pore size distribution in the synthesized BaTiO₃. The nitrogen adsorption-desorption isotherm of BaTiO₃ exhibited hysteresis loop at relative pressure (P/P_0) close to unity is shown in Figure 2 (a), indicating the presence of large mesopores and macropores, which can be ascertained as type IV according to IUPAC classification. This isotherm exhibited H3 hysteresis loop associated with slit like pores.⁹ BET analysis showed that the specific surface area of BaTiO₃ is 15.86 m² g⁻¹. The BJH pore size distribution is broad in the range of 2-100 nm, indicating the presence of mesopores and macropores is shown in Figure 2 (b). This hierarchical meso/macro porous BaTiO₃ nano-hexagons is believed to enhance the photocatalytic activity due to the increasing photo-absorption efficiency and efficient diffusion of molecules caused by the macropores.¹⁰

3.3. Morphology Studies

The morphology of the synthesized BaTiO₃ was studied with the help of electron microscopy. The FESEM images of the BaTiO₃ suggest that the particles have hexagon shape is shown in Figure 3 (a) with red circles. The EDX analysis was carried out for the synthesized BaTiO₃. The EDX spectrum confirms the presence of barium, titanium and oxygen elements is shown in Figure 3 (b). Figure 3 (c) shows the HRTEM image of BaTiO₃. The lattice fringe of about 0.143 nm agrees well with the (220) plane of cubic BaTiO₃ structure. The bright spots of SAED pattern further shows that BaTiO₃ is of single crystalline is shown Figure 3 (d).

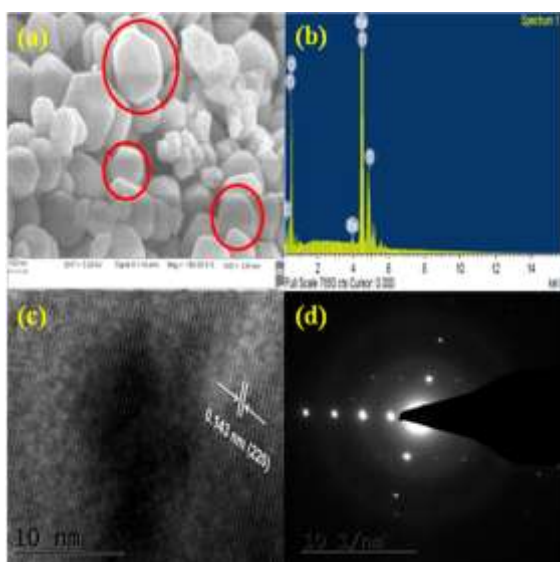
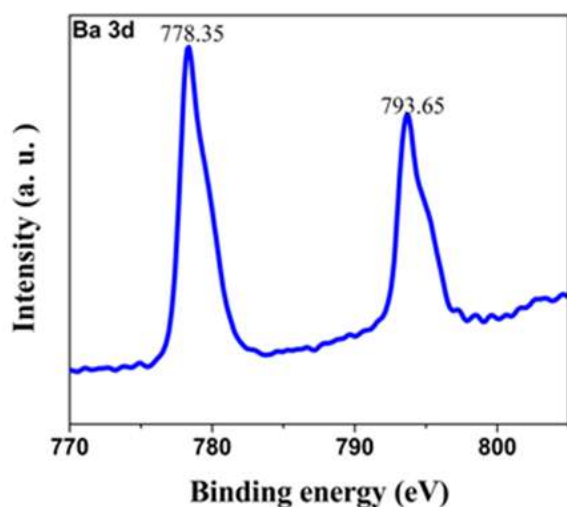


Fig. 3: (a) FESEM image of BaTiO₃ nano-hexagons, (b) EDX spectrum of BaTiO₃, (c) HRTEM image of BaTiO₃, (d) SAED pattern of BaTiO₃

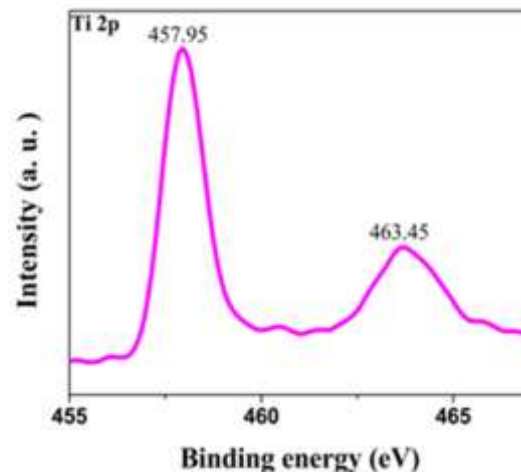
3.4. XPS Analysis

X-ray photoelectron spectroscopy (XPS) measurement was carried out in order to determine the oxidation state and electronic environment of the elements. Figure 4 (a) shows the high-resolution Ba 3d XPS spectrum of BaTiO₃. The two peaks at 793.65 eV and 778.35 eV could be assigned to the splitting of the Ba 3d_{3/2} and Ba3d_{5/2} spin states respectively. Figure 4 (c) shows the narrow scan O 1s XPS spectrum. The two peaks at 529.25 eV and 530.95 eV were assigned to the lattice oxygen (Ti-O bond) and hydroxyl group or adsorbed oxygen in the as synthesized BaTiO₃. Figure 4 (b) shows the narrow scan spectra Ti 2p XPS spectrum. The two peaks at 457.95 eV and 463.45 eV could be ascribed to the splitting of the Ti 2p_{3/2} and Ti 2p_{1/2} spin states respectively.¹¹ The binding energy of Ti 2p_{3/2} is found to be 457.95 eV, which is blue shifted as compared to the reported values for BaTiO₃ bulks. This downshift in the binding energy is mainly ascribed to the formation of Ti³⁺ defects. Some of the Ti⁴⁺ in BaTiO₃ was transformed to Ti³⁺ in order to balance the oxygen vacancies.¹² The existence of these defects was found to boost the absorption of light in the visible region by upshifting the valence band edge.¹³

(a)



(b)



(c)

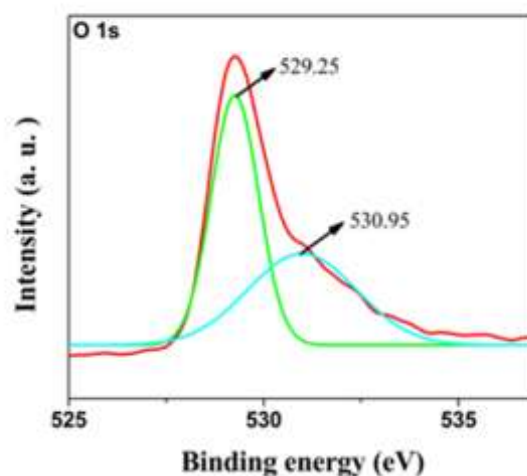


Fig. 4: (a) XPS spectrum of Ba 3d peaks in BaTiO₃, (b) XPS spectrum of Ti 2p peaks in BaTiO₃, (c) XPS spectrum of O 1s peaks in BaTiO₃

3.5. Optical Absorbance Analysis

The band gap is the most crucial factor with respect to the photocatalytic activity of the materials. Figure 5 shows the UV – visible DRS of BaTiO₃. It can be seen that the absorption edge of BaTiO₃ was found to be ca. 426.63 nm. The BaTiO₃ band gap energy was calculated to be 2.90 eV using the relation $E_g = 1240/\lambda$, where λ is the onset absorption wavelength.¹⁴ This result clearly suggest that the BaTiO₃ can perform efficiently as a photocatalyst under visible light.

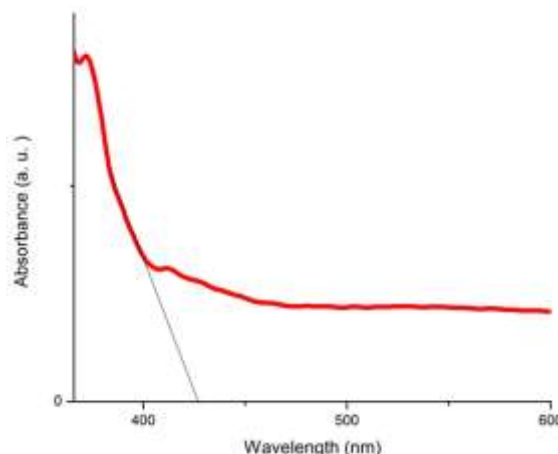


Fig. 5: UV-Vis DRS spectra of BaTiO₃

3.6. Photocatalytic Activity

The photocatalytic activity of BaTiO₃ was evaluated under visible light irradiation by taking methylene blue as a target pollutant. The mixture of MB solution and BaTiO₃ (photocatalyst) was magnetically stirred for 30 minutes in the dark in order to reach adsorption-desorption of the photocatalyst. A blank test was carried out in the absence of photocatalyst, there was no significant degradation. Figure 6 shows the photocatalytic degradation of BaTiO₃. The percentage degradation was found to be 92.8 %.

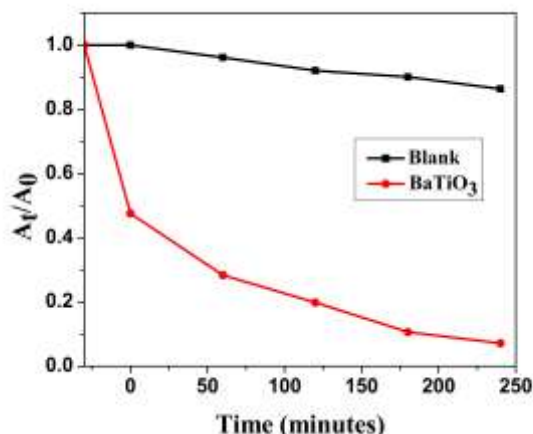


Fig. 6: Degradation rate of MB by BaTiO₃

The photocatalytic degradation of methylene blue by the synthesized BaTiO₃ nano-hexagons followed a pseudo-first order kinetic equation¹⁵ as given in equation (2) is shown in figure 7.

$$\ln(C_t/C_0) = -kt \quad (2)$$

Where, C₀ is the initial concentration, C_t is the concentration at irradiation time (t) and k is the first order rate constant. The rate constant value was measured from the slope of the straight line. The rate constant value was found to be 0.0091

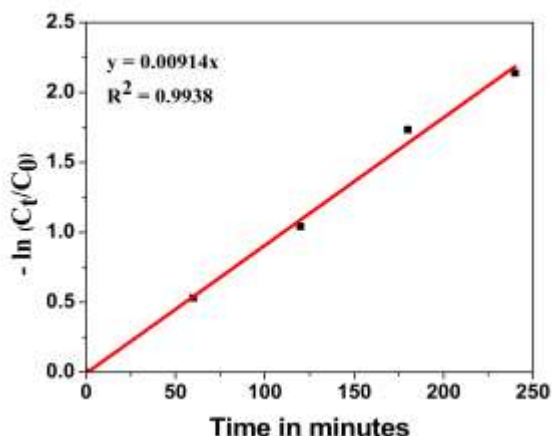


Fig. 7: First order kinetics plot for the photodegradation of MB by BaTiO₃ by visible light irradiation

The reusability of the photocatalysts is another deciding factor for their photocatalytic applications. The stability of the BaTiO₃ nano-hexagons was tested by recycling the photocatalytic experiment. It was found that there is a little loss in the photocatalytic degradation efficiency even after five cycles is shown in figure 8. This indicates that the BaTiO₃ nano-hexagons possess enough stability towards photocatalytic degradation reactions.

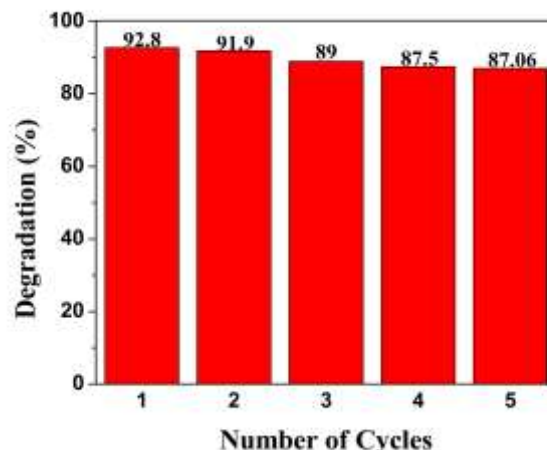


Fig. 8: Recyclability of BaTiO₃ for the degradation of MB under visible light irradiation

3.7 Mechanism of Photocatalytic Activity

The enhanced photocatalytic activity of the BaTiO₃ can be mainly attributed to the efficient photo absorption in the visible region and the efficient generation, separation and migration of the photo-induced charges to the surface of BaTiO₃. The valance band (VB) edge position and the conduction band (CB) position of the BaTiO₃ were calculated with the help of the Mulliken electronegativity theory¹⁶ following eqn. (3) and (4)

$$E_{VB} = \chi - E^\circ + 0.5 E_g \quad (3)$$

$$E_{CB} = E_{VB} - E_g \quad (4)$$

Where E_{VB} is the VB edge potential, E_{CB} is the CB edge potential, E_g is the energy band gap of the semiconductor, χ is the absolute electronegativity of the semiconductor which is calculated as the geometric mean of the electronegativity of the constituent atoms and E^o is the energy of free electrons on the hydrogen scale (-4.5 eV). E_{VB} and E_{CB} of BaTiO₃ were calculated and listed in Table 1.

Table 1. E_{VB} and E_{CB} of BaTiO₃

Sample	χ (eV)	E _g (eV)	E _{VB} (eV)	E _{CB} (eV)
BaTiO ₃	5.27	2.90	2.22	-0.68

3.8 Degradation Mechanism

When the BaTiO₃ nano-hexagons are irradiated with a visible light of energy equal to 2.90 eV, electrons present in the valance band move to the newly formed Ti³⁺ state. As shown in figure 9, the generated electrons probably reacted with dissolved oxygen molecules to form superoxide radical anions (O₂⁻), which on protonation resulted in the formation of hydroperoxy radical (OOH[•]), which finally resulted in the formation of hydroxyl radicals (OH[•]). On the other hand, the generated holes will react with MB or react with surface adsorbed water to generate hydroxyl radicals. The formed hydroxyl radical was a strong oxidizing agent to decompose the organic dyes to harmless products.

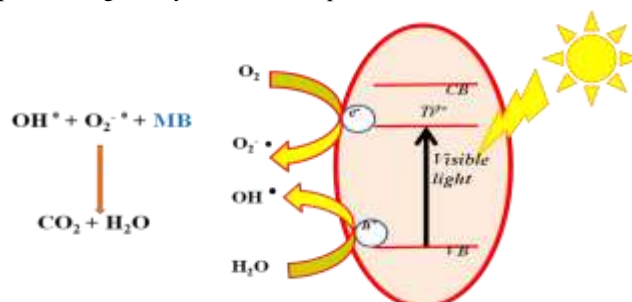


Fig. 9: Mechanism of photodegradation of MB by BaTiO₃ under visible light irradiation

The improvement in the photocatalytic activity of BaTiO₃ under visible light might be due to the special morphology of BaTiO₃ as well as formed Ti³⁺ defects. The morphology control of semiconductors enables selective exposure of photocatalytically active facets, which might be applicable in the design of highly efficient visible light active catalysts. The existence of Ti³⁺ defects or oxygen vacancies was found to boost the absorption of light in the visible region by upshifting the valance band edge. However, an ideal concentration of oxygen vacancies is required to enhance the photocatalytic activity.

4. Conclusion

Hierarchical porous BaTiO₃ nano-hexagons was synthesized successfully by one pot simple hydrothermal route by using TiO₂ and Ba(OH)₂·8H₂O as starting materials under alkaline environment and its photocatalytic activity was evaluated under visible light by taking methylene blue (MB) as a target pollutant. The structural, surface morphological and optical properties of the as prepared BaTiO₃ was characterized by powder X-ray diffraction (XRD), X-ray photoelectron spectroscopy (XPS), field emission scanning electron microscopy (FESEM), energy dispersive X-rays analysis (EDX), high resolution transmission electron microscopy (HRTEM), Brunauer-Emmett-Teller (BET) analysis and diffused reflectance spectroscopic (DRS) techniques. It is noted that the BaTiO₃ nano-hexagons exhibited significant photocatalytic activity towards the degradation of MB under visible light irradiation. This significant photocatalytic activity of BaTiO₃ under visible light is mainly attributed to the special morphology and formation of Ti³⁺ defects. The BaTiO₃ showed high activity as well as high stability even after 5 cycles of photocatalytic processes. The observed results confirmed that the synthesized BaTiO₃ nano-hexagons can be a potential and eco-friendly photocatalyst under visible light.

Acknowledgement

HB is thankful to the National Institute of Technology Surathkal for providing research facilities and financial assistance in the form of an institute fellowship.

References

- [1] R. Vinu & G Madras (2010), Environmental remediation by photocatalysis. *Journal of the Indian Institute of Science* 90, 189-230.
- [2] Y. Wang, C. G. Niu, L. Wang, Y. Wang, X. G. Zhang & G. M. Zheng (2016), Synthesis of fern-like Ag/AgCl/CaTiO₃ plasmonic photocatalysts and their enhanced visible-light photocatalytic properties. *RSC Advances* 6, 47873-47882.
- [3] C. K. Chen, S. X. Zhao, Q. L. Lu, K. Luo, X. H. Zhang & C. W. Nan (2017), Topochemical synthesis and photocatalytic activity of 3D hierarchical BaTiO₃ microspheres constructed from crystal-axis-oriented nanosheets. *Dalton Transactions* 46, 5017-5024.
- [4] Y. Bi, S. Ouyang, N. Umezawa, J. Cao & J. Ye (2011), Facet Effect of Single-Crystalline Ag₃PO₄ Sub-microcrystals on Photocatalytic Properties. *Journal of American Chemical Society* 133, 6490-6492.
- [5] X. Yan, X. Huang, Y. Fang, Y. Min, Z. Wu, W. Li, J. Yuan & L. Tan (2014), Synthesis of Rodlike CaTiO₃ with Enhanced Charge Separation Efficiency and High Photocatalytic Activity. *International Journal of Electrochemical Science* 9, 5155-5163.
- [6] X. Xiong, R. Tian, X. Lin, D. Chu & S. Li (2015), Formation and Photocatalytic Activity of BaTiO₃Nanocubes via Hydrothermal Process. *Journal of Nanomaterials* 2015, 1-6.
- [7] P. Saikia, A. T. Miah & P. P. Das (2017), Highly efficient catalytic reductive dehydration of various organic dyes by Au/Ce-TiO₂ nano-hybrid. *Journal of Chemical Sciences* 129, 81-93.
- [8] M. M. J. Sadiq, U. S. Shenoy & D. K. Bhat (2016), Novel RGO-ZnWO₄-Fe₃O₄ nanocomposite as high performance visible light photocatalyst. *RSC Advances* 6, 61821-61829.
- [9] Q. Xiang, J. Yu & M. Jaroniec (2011), Enhanced photocatalytic H₂- production activity of graphene-modified titania nanosheets. *Nanoscale* 3, 3670-3678.
- [10] Y. Kobayashi, T. Nozaki, R. Kanasaki, R. Shoji & K. Sato (2017), Fabrication of Macroporous TiO₂ Loaded with Magnetite for Photocatalytic Degradation of Methylene Blue. *Journal of Chemical Engineering Japan* 50, 132-135.
- [11] W. W. Lee, W. H. Chung, W. S. Huang, W. C. Lin, W. Y. Lin, Y. R. Jiang & C. C. Chen (2013), Photocatalytic activity and mechanism of nano-cubic barium titanate prepared by a hydrothermal method. *Journal of Taiwan Institute of Chemical Engineers* 44, 660-669.
- [12] Y. Yang, X. Wang, C. Sun & L. Li (2009), Structure study of single crystal BaTiO₃ nanotube arrays produced by the hydrothermal method. *Nanotechnology* 20, 1-5.
- [13] M. Liu, X. Qiu, M. Miyauchi & K. Hashimoto (2011), Cu(II) Oxide Amorphous Nanoclusters Grafted Ti³⁺ Self-Doped TiO₂: An Efficient Visible Light Photocatalyst. *Chemistry of Materials* 23, 5282-5286.
- [14] L. Zhang, Y. Li, Q. Zhang & H. Wang (2013), Hierarchical nanostructure of WO₃ nanorods on TiO₂nanofibers and the enhanced visible light photocatalytic activity for degradation of organic pollutants. *CrystEngComm*, 15, 5986-5993.
- [15] M. M. J. Sadiq, U. S. Shenoy & D. K. Bhat (2017), NiWO₄-ZnO-NRGO ternary nanocomposite as an efficient photocatalyst for degradation of methylene blue and reduction of 4-nitro phenol. *Journal of Physics and Chemistry of Solids* 109, 124-133.
- [16] M. M. J. Sadiq, U. S. Shenoy & D. K. Bhat (2017), Enhanced photocatalytic performance of N-doped RGO-FeWO₄/Fe₃O₄ ternary nanocomposite in environmental applications. *Materials Today Chemistry* 4, 133-141.